OPTIMIZATION OF IBUPROFEN AND CIPROFLOXACIN LOADING ON INORGANIC 2D LAYERED MATERIALS VIA RESPONSE SURFACE METHODOLOGY (RSM)-CENTRAL COMPOSITE DESIGN (CCD) AND APPLICATION FOR ANTIBACTERIAL AND ANTI-INFLAMMATORY

Đến tòa soạn: 21-05-2025

Ngo Thi Tuong Vy[1,2], Dang Nguyen Nha Khanh[2], Le Ngoc Thuy Trang[2], Doan Thi Minh Phuong[3], Nguyen Thi Kim Phuong[1,2]*

[1] *Graduate University of Science and Technology, VAST, Hanoi, Vietnam*

[2] *Institute of Advanced Technology, VAST, Ho Chi Minh City, Vietnam*

[3] *Faculty of Chemical Engineering, Ho Chi Minh City University of Industry and Trade, Ho Chi Minh City, Vietnam*

**E-mail: nguyenthikimp@yahoo.ca*

TÓM TẮT

TỐI ƯU HÓA NẠP LIỆU IBUPROFEN VÀ CIPROFLOXACIN TRÊN VẬT LIỆU LỚP 2D VÔ CƠ THÔNG QUA PHƯƠNG PHÁP BỀ MẶT PHẢN ỨNG (RSM) - THIẾT KẾ PHỐI HỢP CÓ TÂM (CCD) VÀ ỨNG DỤNG KHÁNG KHUẨN, KHÁNG VIÊM

Nghiên cứu này tập trung chế tạo các mẫu CIP-ZnAl-LDH và IBU-ZnAl-LDH dựa trên quá trình tối ưu hóa sử dụng phương pháp bề mặt đáp ứng (RSM) kết hợp với thiết kế phối hợp có tâm (CCD) (trong đó, CIP là thuốc kháng sinh ciprofloxacin, IBU là thuốc chống viêm ibuprofen và ZnAl-LDH là vật liệu hydroxit lớp đôi). Các điều kiện tiên quyết bao gồm nhiệt độ (X_1:70 ℃), thời gian phản ứng (X_2:18 h) và khối lượng CIP (X_3: 1,0 g)/khối lượng IBU (X_3: 0,5 g) để đạt công thức tối ưu (CIP-ZnAl-LDH chứa 41,89% CIP và IBU-ZnAl-LDH chứa 27,51 % IBU). Về tiềm năng kháng khuẩn, giá trị nồng độ ức chế tối thiểu (MIC) của CIP-ZnAl-LDH đối với E. coli và B. subtilis là 100 µg/mL và vùng ức chế đạt 22 mm đối với E. coli và 19 mm đối với B. subtilis. Về độc tính tế bào, IBU-ZnAl-LDH chỉ biểu hiện độc tính tế bào ở nồng độ cao (100 µg/mL). Sử dụng CIP-ZnAl-LDH (10-100 µg/mL) và IBU-ZnAl-LDH (10-30 µg/mL) để đảm bảo hơn 80 % tỷ lệ sống của tế bào RAW 264.7.

Từ khóa: *ZnAl-LDH, Ciprofloxacin, Ibuprofen, phương pháp bề mặt đáp ứng, thiết kế phối hợp có tâm, kháng khuẩn và độc tính tế bào*

1. INTRODUCTION

Advanced material-based drug delivery technology has opened up new opportunities for therapeutics as these materials can maintain therapeutic drug concentrations, minimize side effects, enhance drug efficacy, etc. [1]. As a two-dimensional nanostructured inorganic layered material, layered double hydroxide (LDHs) was considered a novel and promising candidate for the development of drug delivery systems because of its good biocompatibility and low cytotoxicity, high drug loading capacity, and protection of loaded drugs from degradation [1]. In addition to the requirement of good drug carriers, optimizing the drug loading efficiency on LDHs was very important to accelerate the process of killing bacteria effectively and without causing side effects. The conventional and classical approach based on the selection of one factor at a time

was comprehensive but time-consuming and infeasible to derive realistic optimal conditions and interactions between factors [2]. Statistical experimental design was a method characterized by varying factors simultaneously at different levels, thereby finding the main effects and interactions between factors using the minimum number of experiments without compromising the quality [3]. This study used response surface methodology with central composite design (RSM-CCD) to optimize the loading efficiency of antibiotic (Ciprofloxacin-CIP) and anti-inflammatory drug (Ibuprofen-IBU) onto ZnAl-LDH to find the desired constraints along with the interactions between factors such as temperature, time and drug mass. Furthermore, the CIP-LDH and IBU-LDH samples were also characterized and applied for antibacterial and cytotoxicity.

2. EXPERIMENT

2.1. Statistical design for drug loading onto ZnAl-LDH

RSM-CCD statistical modeling was used to optimize drug loading efficiency (CIP or IBU) onto ZnAl-LDH two-dimensional materials. Using Design Expert Version 13.0.5.0 (Stat-Ease Inc., Minneapolis, USA), 17 experimental runs were generated to examine the effects of three factors including temperature (X_1), reaction time (X_2), CIP/IBU mass (X_3) on the loading efficiency of each drug onto ZnAl-LDH. The levels of the three factors were coded as – 1 (low), 0 (medium), and + 1 (high). The value ranges for X_1, X_2, and X_3 were 55-75 °C, 16-19 h, and 0.5-1.0 g for CIP or 0.25-0.5 g for IBU, respectively. The mass of ZnAl-LDH was kept constant at 1.0 gram in all experiments. Each experimental run used a quadratic design to quantify the response and regression analysis. The model is statistically significant if the *p*-value is less than 0.05 (95 % confidence level). The mathematical relationship between the response and the independent variables can be modeled using the following quadratic model:

$$Y = \sum_{i=1}^{3} b_i X_i + \sum_{i=1}^{3} b_{ii} X_i^2 + \sum_{i \neq j, i=1, j=2}^{3} b_{ij} X_i X_j + b_0 \quad (1)$$

where Y is the response; X_i and X_i^2 are the independent variables and quadratic parameters, respectively; $X_i X_j$ is the interaction of the independent variables; b_0 is the intercept coefficient and b_i, b_{ii}, b_{ij} are the linear coefficients.

2.2. Drug loading onto the ZnAl-LDH

The experiments on the synthesis of ZnAl-LDH and drug loading onto ZnAl-LDH were performed in an ultrasonic bath under N_2 atmosphere. The solution (0.75 M $Zn(NO_3)_2$ and 0.25 M $Al(NO_3)_3$) was added dropwise into the alkaline solution (2 M NaOH and 0.2 M Na_2CO_3), ultrasonicated at 100 W. The pH of the solution was maintained at 10 throughout the synthesis. The resulting slurry (ZnAl-LDH) was aged at 70 °C and 100 W ultrasonicated for 24 h. The solid was collected by centrifugation, followed by washing with deionized water and drying at 70 °C for 10 h and calcination at 520 °C for 3 h to obtain ZnAl-LDO.

Approximately 1.0 g of finely ground ZnAl-LDO was dispersed in 250 mL of solution containing 0.5-1.0 g of CIP or 0.25-0.5 g of IBU and ultrasonicated at 100 W. The temperature and reaction time were changed to 55-75 °C and 16-19 h,

respectively. The solid products were obtained by filtration, washed with decarbonized distilled water and dried for 18 h at 70 °C. The percentage of CIP or IBU loading on ZnAl-LDH was quantified by measuring the concentration of organic carbon (TOC) in ZnAl-LDH after drug loading. The drug loaded onto ZnAl-LDH expressed as loading efficiency (%LE) was calculated by the following formula:

$$\%LE = \frac{\text{Drug in ZnAl–LDH}}{\text{Mass of product}} \times 100\% \quad (2)$$

2.3. Validation of experimental design

Validation of the experimental design was performed based on relative error (%RE) using the following formula:

$$\%RE = \frac{Predicted\ values - Actual\ values}{Predicted\ values} \times 100\%)$$

2.4. Characterization

The crystal structure and functional groups of the samples were performed on a XRD-6000 X-ray diffractometer (Shimadzu, Tokyo, Japan) and a Bruker Vector 22 FT-IR spectrometer, respectively. The surface morphology of the samples was studied by field emission scanning electron microscopy (FESEM, Hitachi S-4800, Japan). The sample's particle size distribution was determined by Dynamic Light Scattering (DLS) using a Horiba SZ-100 Nanoparticle Analyzer. The elemental composition of the samples was analyzed on a CHNSO elemental analyzer (Mettler Toledo, USA) for organic elements (C, H, O and N), ICP-OES (Perkin Elmer, USA) for Zn, Al and ion chromatography (IC) (Metrohm, Switzerland) for F.

2.5. Antimicrobial activity assay

Standardized strains American Type Culture Collection (ATCC) (Manassas, USA), *Bacillus subtilis* (*B. subtillis* ATCC 6633) and *Escherichia coli* (*E. coli* ATCC 8739) were used to evaluate the antibacterial activity of the materials. For the assays, samples were diluted with dimethyl sulfoxide (DMSO) and loaded into a microtiter plate with each of the microbial strains. Bacterial strains were inoculated in Mueller Hinton medium (MHB, Sigma) for 24 h at 37 °C. Gentamycin and doxycycline were used as positive controls for *E. coli* and *B. subtillis*, respectively. Bacterial strains cultured without gentamycin/doxycycline/ZnAl-LDH/CIP-LDH were used as negative controls. The minimum inhibitory concentration (MIC) is the concentration at which microbial growth could not be seen. Bacterial strains were seeded in 96-well plates and inoculated with different concentrations of CIP, ZnAl-LDH or CIP-LDH (200, 100, 50, 25.5, and 12.5 µg/mL). MIC was determined by visual inspection after inoculation at 37 °C for 24 h. Samples were considered to have antimicrobial activities if the MIC value is ≤ 200 µg/mL.

For the inhibition zone test of the material, sterile Mueller-Hinton agar was prepared on 150 × 15 mm petri dishes. A swab of pure bacterial culture was spread evenly on Mueller-Hinton agar plates. The treated product sample was placed on the medium plates using sterile forceps. These petri dishes were incubated for 24 hours at 37 °C along with other optimal conditions for bacterial growth. After the incubation period, a clear area (zone of inhibition) around the antibacterial product sample was observed and measured.

2.6. Cytotoxicity assays

The assay was conducted to assess the cytotoxicity in the presence of samples (ZnAl-LDH, CIP-LDH and IBU-LDH). RAW 264.7 cells from ATCC (Manassas, VA, USA) were cultured for 48 hrs. in Dulbecco's Modified Eagle Medium (DMEM) and 10% Fetal bovine serum (FBS) at 37 °C in a humidified incubator with 5 % CO_2. RAW264.7 cells were seeded in 96-well plates at a density of 2.5×10^5 cells/well. Cells were then stimulated with 2 µL Lipopolysaccharide (LPS) (0.1 mg/mL) in the presence of samples at concentrations of 10, 30, and 100 µg/mL, and then incubated for 48 hrs. The cells were seeded with cardamonin (0.3 and 3 µM) as a positive control.

After 48 hrs. of incubation of RAW264.7 cells with samples (10-100 µg/mL), the suspension was collected and the NO concentration was determined using Griess reagent (sulfanilic acid and N-1-napthylethylenediamine dihydrochloride (NED) in phosphoric acid medium). Griess reagent (20 µL) was added to 280 µL of the solution mixture (150 µL of the analytical sample and 130 µL of deionized water). Sulfanilic acid reacted with nitrite in an analytical sample to form a diazonium salt, which then reacted with NED to form the azo dye. The absorbance was measured within 30 min. on an Infinite F50 spectrophotometer (Tecan, Männedorf, Switzerland) at 570 nm.

Cell viability was determined using 3-(4,5-Dimethylthiazol-2-yl)-2,5-diphenyltetrazolium bromide (MTT) reagent. After 48 hrs. of incubation of RAW264.7 cells with samples (10-100 µg/mL), the supernatant was replaced with MTT reagent (0.5 mg/mL) and incubated at 37°C for 4 h. After incubation, the MTT reagent was replaced with DMSO solvent. The absorbance of formazan generated from MTT was measured on an Infinite F50 instrument (Tecan, Männedorf, Switzerland) at 540/720 nm. Cell viability (%) was calculated using the following formula:

$$\%\ \text{Viability} = \frac{Absorbance_{sample}}{Absorbance_{Control(-)}} \times 100\% \quad (4)$$

3. RESULTS AND DISCUSSION

3.1. Optimization of drug loading onto ZnAl-LDH

The effects of specific variables and interactions between variables to achieve maximum loading efficiency of CIP or IBU were studied using CCD. A total of 17 experimental runs were performed and the observed results were listed in Table 1. The loading efficiency of CIP and IBU ranged from 31.13 to 41.58 % and 17.33 to 27.19 %, respectively. The experimental data in Table 2 showed a good fit with the quadratic model. The quadratic mode was shown in Equations (5) and (6) describe the relationship between the temperature (X_1), reaction time (X_2) and mass of CIP or IBU (X_3) and loading efficiency (Y) of CIP or IBU onto ZnAl-LDH.

$$Y_{CIP\ loaded} = 0.53X_1 + 0.44X_2 + 3.87X_3 - 1.05X_1^2 - 1.10X_2^2 + 0.66X_3^2 + 0.12X_1X_2 + 0.17X_1X_3 + 0.22X_2X_3 + 36.90 \quad (5)$$

$$Y_{IBU\ loaded} = 1.59X_1 + 0.85X_2 + 1.76X_3 - 3.69X_1^2 - 1.04X_2^2 - 0.90X_3^2 + 0.44X_1X_2 + 0.68X_1X_3 - 0.41X_2X_3 + 26.24 \quad (6)$$

Table 1. *Experimental runs projected and their observed responses*

No.	Variables levels			CIP-LDH			IBU-LDH		
	Temp (°C) (X_1)	Time (h) (X_2)	Mass of CIP/IBU (g) (X_3)	Observed (mean ± SD, n=3)		Predicted	Observed (mean ± SD, n=3)		Predicted
				TOC in product (mg/mg)	% CIP loading	% CIP loading	TOC in product (mg/mg)	% IBU loading	% IBU loading
1	55	16.0	0.50/0.25	0.192 ± 0.009	31.13 ± 1.50	31.09	0.131 ± 0.011	17.33 ± 1.47	17.12
2	75	16.0	0.50/0.25	0.194 ± 0.010	31.52 ± 1.63	31.54	0.138 ± 0.012	18.20 ± 1.64	18.06
3	55	19.0	0.50/0.25	0.193 ± 0.009	31.38 ± 1.45	31.28	0.142 ± 0.012	18.71 ± 1.56	18.77
4	75	19.0	0.50/0.25	0.199 ± 0.010	32.27 ± 1.58	32.23	0.162 ± 0.012	21.40 ± 1.54	21.46
5	55	16.0	1.0/0.5	0.234 ± 0.011	38.00 ± 1.78	38.04	0.153 ± 0.012	20.20 ± 1.64	20.11
6	75	16.0	1.0/0.5	0.241 ± 0.009	39.09 ± 1.46	39.19	0.181 ± 0.011	23.87 ± 1.47	23.77
7	55	19.0	1.0/0.5	0.241 ± 0.009	39.13 ± 1.49	39.11	0.151 ±0.012	20.00 ± 1.57	20.11
8	75	19.0	1.0/0.5	0.251 ± 0.010	40.71 ± 1.55	40.75	0.192 ± 0.010	25.35 ± 1.34	25.52
9	55	17.5	0.750/0.375	0.217 ± 0.008	35.20 ± 1.34	35.33	0.158 ± 0.009	20.82 ± 1.19	20.96
10	75	17.5	0.750/0.375	0.225 ± 0.010	36.50 ± 1.66	36.38	0.183 ± 0.013	24.13 ± 1.68	24.14
11	65	16.0	0.750/0.375	0.219 ± 0.011	35.47 ± 1.75	35.36	0.180 ± 0.011	23.81 ± 1.45	24.35
12	65	19.0	0.750/0.375	0.223 ± 0.010	36.12 ± 1.63	36.24	0.200 ± 0.012	26.45 ± 1.60	26.05
13	65	17.5	0.50/0.25	0.207 ± 0.009	33.53 ± 1.52	33.69	0.177 ± 0.010	23.34 ± 1.36	23.58
14	65	17.5	1.0/0.5	0.256 ± 0.012	41.58 ± 1.92	41.43	0.206 ± 0.011	27.19 ± 1.41	27.10
15	65	17.5	0.750/0.375	0.228 ± 0.012	37.00 ± 1.91	36.90	0.199 ± 0.010	26.31 ± 1.36	26.24
16	65	17.5	0.750/0.375	0.227 ± 0.009	36.90 ± 1.53	36.90	0.197 ± 0.011	26.05 ± 1.41	26.24
17	65	17.5	0.750/0.375	0.227 ± 0.009	36.82 ± 1.43	36.90	0.202 ± 0.008	26.66 ± 1.10	26.24

The 3D graph in Fig. 1 showed that CIP and IBU loading efficiency was positively influenced by all the three processing parameters. Equation 5 presents that temperature and reaction time had a negligible influence on CIP loading efficiency compared to CIP mass. The CIP loading efficiency increased with increasing CIP mass (Figure 1b and 1c). Equation 6 presents temperature and IBU mass had a greater impact on the IBU loading efficiency than time. When temperature and IBU mass increased, IBU loading efficiency was also increased. The ANOVA results for the quadratic model (Equations 5 and 6) were presented in Table 2.

For the CIP loading efficiency on ZnAl-LDH, the coefficient of determination fits the data relatively well, with a high R^2 value of 0.9991 and an adjusted R^2 value of 0.9979, which implied that the model could accurately predict the CIP loading efficiency on ZnAl-LDH. The coefficient of variation (C.V.) is 0.41 %, which was within the acceptable range (<10 %) [4],

implying that the proposed model was a good fit. Adequate precision of 92.06, which was much higher than the desired value (desired > 4), implied that this model could be used to navigate the design space. The statistical significance of the coefficient terms was evaluated through the *p*-values ($p < 0.05$) and F-values. The high F-value (F = 856.51) and low *p*-value (<0.0001) (Table 2) demonstrated that the model was highly significant. For the main effects, the CIP mass (X_3) had a significant effect on the CIP loading efficiency onto ZnAl-LDH (F = 6976.17, $p < 0.0001$), followed by temperature (X_1) (F = 128.52, $p < 0.0001$), while reaction time (X_2) had a lower effect but still significant (F = 90.27, $p < 0.0001$). Furthermore, the interaction between reaction time (X_2) and CIP mass (X_3) had a more significant effect (high F of 17.85 and p = 0.0039) compared to the other interactions. The order of the independent variables to enhance the CIP loading efficiency onto ZnAl-LDH was $X_3 >> X_1 > X_2$, while the order of the interaction variables was $X_2X_3 > X_1X_3 > X_1X_2$.

Table 2. *ANOVA result for loading efficiency of CIP or IBU onto ZnAl-LDH*

Source of variation	CIP-LDH				IBU-LDH			
	Sum of squares	Degrees of freedom	F-value	*p*-value	Sum of squares	Degrees of freedom	F-value	*p*-value
Model	165.32	9	856.51	< 0.0001	168.22	9	147.87	< 0.0001
X_1	2.76	1	128.52	< 0.0001	25.25	1	199.76	< 0.0001
X_2	1.94	1	90.27	< 0.0001	7.23	1	57.16	0.0001
X_3	149.61	1	6976.17	< 0.0001	31.08	1	245.90	< 0.0001
X_1^2	2.95	1	137.71	< 0.0001	36.49	1	288.70	< 0.0001
X_2^2	3.27	1	152.52	< 0.0001	2.87	1	22.73	0.002
X_3^2	1.15	1	53.61	0.0002	2.17	1	17.19	0.0043
X_1X_2	0.1225	1	5.71	0.0482	1.53	1	12.11	0.0103
X_1X_3	0.2415	1	11.26	0.0122	3.73	1	29.48	0.001
X_2X_3	0.3828	1	17.85	0.0039	1.36	1	10.77	0.0135
Residual	0.1501	7	-	-	0.8848	7	-	-
Lack of Fit	0.1339	5	3.29	0.2493	0.6974	5	1.49	0.4484
Pure Error	0.0163	2	-	-	0.1874	2	-	-
Total Corrected	165.47	16	-	-	169.10	16	-	-
	%C.V = 0.41; Predicted R^2 = 0.9933				*%C.V = 1.55; Predicted R^2 = 0.9662*			
	R^2 = 0.9991; Adjusted R^2 = 0.9979				*R^2 = 0.9948; Adjusted R^2 = 0.9880*			
	Adequate Precision = 92.06				*Adequate Precision = 36.61*			

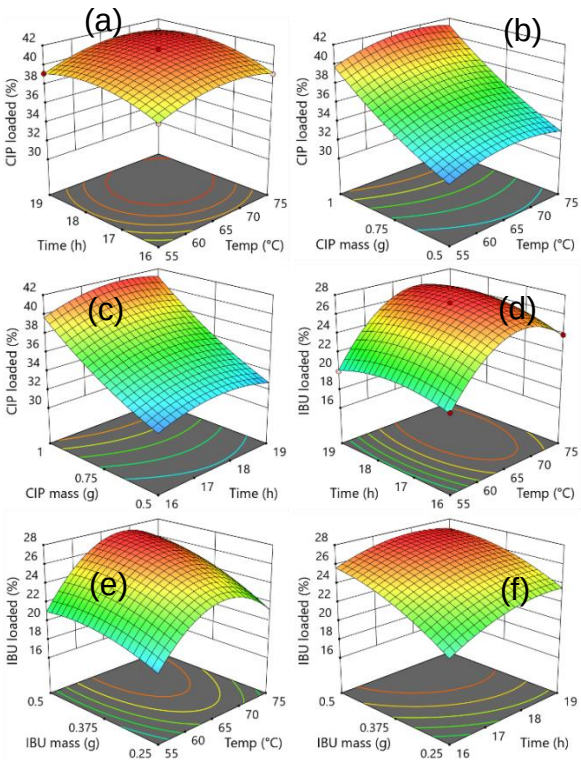

Figure 1. *Response surface plots of CIP (a-c) and IBU (d-f) loading onto ZnAl-LDH at optimum condition*

In the case of IBU, the ANOVA results also showed that the proposed model was a good fit (C.V = 1.55 %) and could accurately predict the IBU loading efficiency onto ZnAl-LDH (R^2 = 0.9948 and adjusted R^2 = 0.9880). Adequate precision of 36.61 showed that the model could navigate the design area. In addition, the model was highly significant (F = 168.22 and $p < 0.0001$). The order of main effects that influenced with the IBU loading efficiency onto ZnAl-LDH was IBU mass (X_3: F = 245.90, $p < 0.0001$) > temperature (X_1: F = 199.76, p < 0.0001) > reaction time (X_2: F = 57.16, p = 0.0001). The order of the interaction variables was X_1X_3 (F = 29.48, p = 0.001) > X_1X_2 (F = 12.11, p = 0.0103) > X_2X_3 (F = 10.77, p = 0.0135).

3.2. Validation Experiments of drug loading efficiency

The CIP-LDH and IBU-LDH samples were prepared based on the optimal conditions including temperature of 70 °C, reaction time of 18 h, and drug mass of 1.0 g for CIP or 0.5 g for IBU to validate the accuracy and reliability of the model. For CIP-LDH, the predicted loading efficiency from the model and the actual loading efficiency were 41.63% and 41.89 ± 1.18 % (n = 3), respectively, with % RE of – 0.62. In the case of IBU-LDH, the predicted and actual loading efficiency were 27.42 % and 27.51 ± 0.68 %, respectively, with % RE of – 0.33. The close agreement between predicted and actual results, with % RE within the acceptable range (< 5 %), emphasized the importance of predictive software in the drug loading process.

3.3. Chemical composition and characterization of optimized CIP-LDH and IBU-LDH

Table 3 presented the results of elemental composition analysis (C, H, O, N, Zn, Al, F) of the ZnAl-LDH, CIP-LDH (41.89 % CIP) and IBU-LDH (27.51 % IBU) samples using CHNSO elemental analyzer, ICP-OES and ion chromatography. Based on the elemental results and the charge balance principle, the predicted empirical formulas were as follows:

- ZnAl-LDH:

$Zn_{1.51}Al_{0.52}(OH)_4(NO_3)_{0.58}.1.31H_2O$

- CIP-LDH:

$Zn_{1.45}Al_{0.5}(OH)_4(C_{17}H_{18}FN_3O_3)_{0.38}$

- IBU-LDH:

$Zn_{1.44}Al_{0.49}(OH)_4\,(C_{13}H_{18}O_2)_{0.35}.\,0.8H_2O$

The calculated results from the predicted

empirical formulas were close to the actual analysis results, indicating that the predicted empirical formula was appropriate.

Table 3. *Results of elemental composition of the samples (values presented as actual/predicted from the formula)*

Element	ZnAl-LDH	CIP-LDH	IBU-LDH
Zn (%)	40.79/40.79	31.67/31.67	35.58/35.58
Al (%)	5.74/5.74	4.48/4.48	5.04/5.04
O (%)	46.57/46.57	26.58/27.51	33.40/33.40
$C_{Organic}$ (%)	-	25.79/25.79	20.83/20.83
N (%)	3.37/3.37	5.31/5.31	-
H (%)	3.32/2.73	3.81/3.62	5.09/4.53
F (%)	-	2.40/2.40	-

As seen in Figure 2a, the XRD pattern of ZnAl-LDH showed sharp and symmetric diffraction peaks, which could be attributed to (003), (006), (012), (009), (015), (018), and (113), corresponding to hydrotalcite-like materials (JCPDS No. 48-1022 and 38–0486) [5-7]. In addition, some diffraction peaks of ZnAl-LDH also matched the crystal planes (100), (300), and (119) of hexagonal $Zn(OH)_2$ (JCPDS No. 48–1066) [8]. The peaks of CIP-LDH and IBU-LDH were similar to those of ZnAl-LDH, however, the loading of CIP and IBU onto ZnAl-LDH broadened the d_{003} basal spacing from 0.76 nm of ZnAl-LDH to 1.61 nm for CIP-LDH and 1.45 nm for IBU-LDH. CIP broadened the d_{003} basal spacing of ZnAl-LDH more than IBU because the three-dimensional size of the CIP molecule ($1.250 \times 0.782 \times 0.396$ nm) [9] was larger than that of IBU ($0.954 \times 0.479 \times 0.407$ nm) [10].

The absorption bands at 3420, 1629 and 1377 cm^{-1} in the FTIR spectrum of ZnAl-LDH were characteristic of the stretching vibration of the OH^- group, the bending vibration of water [5] and the NO_3^- groups (Figure 2b). The loss of proton of the COOH group and the stretching of the C=O bond led to the disappearance of the band at 1706 cm^{-1} and the shift of the band from 1270 cm^{-1} to 1260 cm^{-1} of CIP-LDH compared to CIP. In addition, the FTIR spectrum of CIP-LDH also showed a new absorption band at 1567 cm^{-1}. The change of these bands indicated the presence and interaction between CIP and ZnAl-LDH. Similarly, a significant decrease in the intensity of the band at 1711 cm^{-1}, a shift of the band from 1416 cm^{-1} to 1421 cm^{-1} and the appearance of a new band at 1634 cm^{-1} also occurred for IBU-LDH. The bands at 1567, 1385 cm^{-1} of CIP-LDH and 1634, 1421 cm^{-1} of IBU-LDH were the asymmetric ($\nu_{as}COO^-$) and symmetric (ν_sCOO^-) stretching vibrations of the carboxylate group. The energy splitting $\Delta\nu$ ($\Delta\nu = \nu_{as}COO^- - \nu_sCOO^-$) indicated the type of metal-ligand interaction [11]. The $\Delta\nu$ of CIP-LDH and IBU-LDH were 182 cm^{-1} and 213 cm^{-1}, respectively, which meant that the bonding between CIP and ZnAl-LDH was in the bidentate bridging type and the bonding between IBU and ZnAl-LDH was in the monodentate type [11].

The typical morphology of ZnAl-LDH was agglomerated non-uniform sheets (Figure 2c). The loading of CIP and IBU significantly affected the structural properties of ZnAl-LDH. The drug anion clusters and the ZnAl-LDH host form flat and individually stacked sheets. By bridging bidentate and monodentate

interactions, CIP and IBU were successfully loaded into ZnAl-LDH [12]. DLS results showed that the Z-average of ZnAl-LDH, CIP-LDH and IBU-LDH were 110.2, 216.9 and 235.8 nm, respectively.

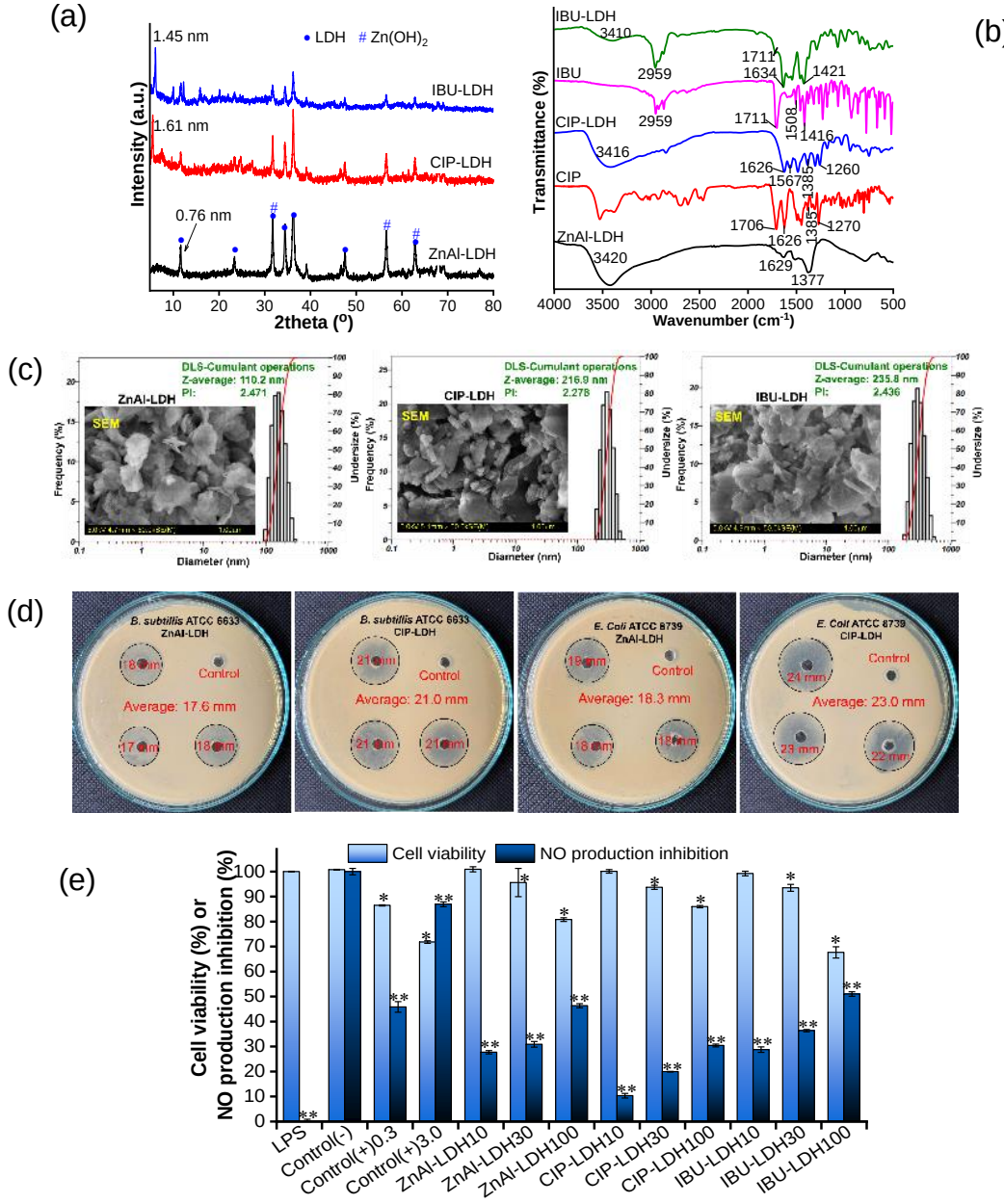

Figure 2. *(a) XRD pattern, (b) FTIR spectra, (c) DLS and FESEM image (inset) of materials, (d) Inhibition zone for ZnAl-LDH (150 µg/mL) and CIP-LDH (100 µg/mL) and (e)Effects of samples on RAW264.7 cells viability and NO production inhibition (mean ± SD, n=3). Significant differences in cell viability (*) and NO production inhibition (**) compared to the control (−) (LSD test, p<0.05)*

3.4. Antibacterial efficacy and Cytotoxicity

According to our previous publication [13], the drug release from CIP-LDH (41.89 % CIP) and IBU-LDH (27.51 % IBU) in phosphate buffer-PBS solution (pH 5.8 and 7.4) lasted for 12 hrs. The release mechanism of CIP from CIP-LDH was drug diffusion and carrier erosion

while the release mechanism of IBU from IBU-LDH was drug diffusion. The sustained drug release process could enhance the antibacterial and anti-inflammatory effects. For the antibacterial efficacy assay, *E. coli* and *B. subtilis* were treated with CIP, ZnAl-LDH and CIP-LDH at different concentrations after being placed in 96-well plates and incubated at 37°C for 24 hrs. The minimum inhibitory concentration (MIC) value of CIP against *E. coli* and *B. subtilis* was found to be 200 µg/mL, while the MIC of ZnAl-LDH and CIP-LDH against these bacterial strains was 150 and 100 µg/mL, respectively. The antibacterial property of ZnAl-LDH could be considered as an additional advantage for use as a drug carrier. Previous studies also showed that ZnAl-LDH exhibited good antibacterial activity, with very few bacterial colonies found in the presence of ZnAl-LDH (Zn:Al = 4:1) [14]. In addition, the antibacterial activity of ZnAl-LDH was enhanced by increasing the molar ratio of Zn-Al [15]. Another recent study also reported the superior antibacterial efficacy of Zn-based materials [16]. As shown in Figure 2d, the inhibition zone of 150 µg/mL ZnAl-LDH reached 18.3 mm for *E. coli* and 17.6 mm for *B. subtilis*, while 100 µg/mL CIP-LDH exhibited larger inhibition zones against these pathogens. The inhibition zone of 100 µg/mL CIP-LDH reached 23 mm for *E. coli* and 21 mm for *B. subtilis*. The antibacterial effect of CIP-LDH might be due to the synergistic effect between CIP and ZnAl-LDH.

Regarding cytotoxic effects, RAW264.7 cells were cultured with ZnAl-LDH, CIP-LDH and IBU-LDH at different concentrations (10–100 µg/mL) for 48 hrs. The results from MTT assay indicated that the effect of these samples on the viability of RAW264.7 cells was concentration dependence. Significant reduction in cell viability compared to the negative control group was found at higher concentrations of the samples (30–100 µg/mL) while lower concentrations (10 µg/mL) had no effect (Figure 2e). More than 80% RAW 264.7 macrophage viability was found in the group treated with ZnAl-LDH and CIP-LDH (10–100 µg/mL), which indicated that ZnAl-LDH and CIP-LDH were less toxic. The low cytotoxicity of ZnAl-LDH was considered an advantage to serve as a carrier and delivery for drugs. In contrast, more than 67% viability RAW 264.7 macrophages were found in the groups treated with IBU-LDH at 100 µg/mL, respectively. Thus, to avoid cytotoxic effects and allow at least 80% cell survival, the appropriate concentration of IBU-LDH used to determine the anti-inflammatory effect should be below 100 µg/mL.

The anti-inflammatory activity of ZnAl-LDH, CIP-LDH and IBU-LDH was demonstrated by the inhibition of NO production in LPS-stimulated RAW 264.7 cells. The results in Figure 1 showed that ZnAl-LDH, CIP-LDH and IBU-LDH at various concentrations significantly inhibited NO production compared with the control groups. As shown in Figure 2e, the positive control group (stimulated with 0.1 mg/mL LPS) had a 0 % inhibition of NO production and the negative control group (without stimulation with 0.1 mg/mL LPS) had a 100% inhibition of NO production. The inhibition of NO production by ZnAl-

LDH, CIP-LDH and IBU-LDH was in a dose-dependent manner. The inhibition of NO production increased with increasing concentrations of the samples. At 100 µg/mL, IBU-LDH showed the greatest inhibitory effect on NO production of 51 %, followed by ZnAl-LDH and CIP-LDH of 46% and 30 %, respectively. The concentrations of ZnAl-LDH and CIP-LDH required to inhibit 50 % of NO formation (IC_{50}) were greater than 100 µg/mL while the IC_{50} of IBU-LDH was about 98 µg/mL.

4. CONCLUSION

The three-level-three-factor CCD-RSM was used to optimize the drugs loading efficiency on ZnAl-LDH. The prerequisites included temperature (X_1:70 °C), reaction time (X_2:18 h) and CIP mass (X_3: 1.0 g)/IBU mass (X_3: 0.5 g) to achieve the optimal formulation (CIP-LDH contains 41.89 % CIP and IBU-LDH contains 27.51 % IBU). The successful loading of CIP and IBU onto ZnAl-LDH widened the d_{003} basal spacing from 0.76 nm of ZnAl-LDH to 1.61 nm for CIP-LDH and 1.45 nm for IBU-LDH. Regarding the antibacterial potential, the MIC value of CIP-LDH against *E. coli* and *B. subtilis* was 100 µg/mL and the inhibition zone reached 23 mm for *E. coli* and 21 mm for *B. subtilis*. Regarding the cytotoxicity, IBU-LDH exhibited cytotoxicity only at high concentrations (100 µg/mL). Using CIP-LDH (10-100 µg/mL) and IBU-LDH (10-30 µg/mL) could ensure the survival rate of RAW 264.7 cells above 80 %. The IC_{50} value of ZnAl-LDH and CIP-LDH is greater than 100 µg/mL while the IC_{50} of IBU-LDH was 98 µg/mL.

REFERENCES

[1] V. Rives, M. del Arco, C. Martín, (2013). Layered double hydroxides as drug carriers and for controlled release of non-steroidal antiinflammatory drugs (NSAIDs): A review. *Journal of Controlled Release* **169**, 28-39.

[2] A. Ćurić, R. Reul, J. Möschwitzer, G. Fricker, (2013). Formulation optimization of itraconazole loaded PEGylated liposomes for parenteral administration by using design of experiments. *International Journal of Pharmaceutics* **448**, 189-197.

[3] K. Preeti, M. Jitender, K. Parveen, (2019). Application of central composite design and response surface methodology for optimization of metal organic framework: novel carrier for drug delivery. *Asian Journal of Pharmaceutical and Clinical Research* **12**, 121-127.

[4] J. Wu, H. Zhang, N. Oturan, Y. Wang, L. Chen, M. A. Oturan, (2012). Application of response surface methodology to the removal of the antibiotic tetracycline by electrochemical process using carbon-felt cathode and DSA (Ti/RuO2–IrO2) anode. *Chemosphere* **87**, 614-620.

[5] X. Q. Zhang, M. G. Zeng, S. P. Li, X. D. Li, (2014). Methotrexate intercalated layered double hydroxides with different particle sizes: structural study and controlled release properties. *Colloids and Surfaces B: Biointerfaces* **117**, 98-106.

[6] A. Li, H. Deng, C. Ye, Y. Jiang, (2020). Fabrication and Characterization of Novel ZnAl-Layered Double Hydroxide for the Superadsorption of Organic Contaminants from Wastewater. *ACS Omega* **5**, 15152-15161.

[7] A. Grover, R. Kaur, I. Mohiuddin, A. K. Malik, J. S. Aulakh, Y. F. Tsang, K.-H. Kim, (2019). Surfactant-modified Zn/Al-layered double hydroxides for efficient

extraction of alkyl phenols from aqueous samples. *Environmental Research* **177**, 108605.

[8] W. Qin, Q. Yang, H. Ye, Y. Xie, Z. Shen, Y. Guo, Y. Deng, Y. Ling, J. Yu, G. Luo, N. Raza, W. Raza, J. Zhao, (2023). Novel 2D/2D BiOBr/Zn(OH)2 photocatalysts for efficient photoreduction CO2. *Separation and Purification Technology* **306**, 122721.

[9] N. A. Lopez, C. V. Luengo, M. J. Avena, (2022). Ciprofloxacin in Layered Double Hydroxides: Looking for the Best Synthesis Method. *Journal of Pharmaceutical Sciences* **111**, 1429-1436.

[10] C. V. Luengo, M. C. Crescitelli, N. A. Lopez, M. J. Avena, (2021). Synthesis of Layered Double Hydroxides Intercalated With Drugs for Controlled Release: Successful Intercalation of Ibuprofen and Failed Intercalation of Paracetamol. *Journal of Pharmaceutical Sciences* **110**, 1779-1787.

[11] Y. A. Barnakov, I. U. Idehenre, S. A. Basun, T. A. Tyson, D. R. Evans, (2019). Uncovering the mystery of ferroelectricity in zero dimensional nanoparticles. *Nanoscale Advances* **1**, 664-670.

[12] V. Yousefi, V. Tarhriz, S. Eyvazi, A. Dilmaghani, (2020). Synthesis and application of magnetic@layered double hydroxide as an anti-inflammatory drugs nanocarrier. *Journal of Nanobiotechnology* **18**, 155.

[13] N. T. T. Vy, D. N. N. Khanh, P. D. Khanh, N. T. Phat, N. T. Anh, N. L. Nguyen, T. N. L. Anh, N. N. Vy, L. T. M. Dan, N. T. K. Phuong, (2023). Drug-Intercalated Zn–Al-Layered Double Hydroxides as Antibacterial and Anti-inflammatory Delivery Systems for Wound Healing Applications. *Journal of Cluster Science* **34**, 2619-2632.

[14] H.-M. Cheng, X.-W. Gao, K. Zhang, X.-R. Wang, W. Zhou, S.-J. Li, X.-L. Cao, D.-P. Yan, (2019). A novel antimicrobial composite: ZnAl-hydrotalcite with p-hydroxybenzoic acid intercalation and its possible application as a food packaging material. *New Journal of Chemistry* **43**, 19408-19414.

[15] M. Lobo-Sánchez, G. Nájera-Meléndez, G. Luna, V. Segura-Pérez, J. A. Rivera, G. Fetter, (2018). ZnAl layered double hydroxides impregnated with eucalyptus oil as efficient hybrid materials against multi-resistant bacteria. *Applied Clay Science* **153**, 61-69.

[16] R. Li, M. Cai, Z. Xie, Q. Zhang, Y. Zeng, H. Liu, G. Liu, W. Lv, (2019). Construction of heterostructured CuFe2O4/g-C3N4 nanocomposite as an efficient visible light photocatalyst with peroxydisulfate for the organic oxidation. *Applied Catalysis B: Environmental* **244**, 974-982.